Study of amphibolite facies metapelites from the Hydrated Zone of the Southern Marginal Zone, Limpopo Belt, South Africa. Petrography and phase equilibria modelling.

Stellenbosch University, South Africa

Student: Hugo Dominguez Carranza

Supervisor: Professor Gary Stevens

Abstract :

The geological history of the Southern Marginal Zone of the Limpopo Belt, in South Africa, is one of the less understood in South Africa and one of the most debated in the recent years. This report is a preliminary work, which, from samples collected in the field, try to better understand the history of the rocks from the Hydrated Zone, by the use of a petrography study, chemical analysis and phase equilibria modelling. Textures and relations of minerals were studied and three generations of garnet were distinguished. The first two are interpreted as granulite facies relics and the third one, as retrograde garnets in the amphibolite facies. PT conditions of ca. 650°C and 8.5 kbar were found for the retrograde event, in agreement with recent published works. The impact of graphite-saturated C-O-H fluids was also investigated on the equilibrium computed, and it was shown that it doesn't impact significantly the models for the PT conditions of interest.

I. Introduction

The global tectonic style during the Archean (4.0-2.5 Gyr) is an enduring enigma. As the Earth was hotter at that time, it is reasonable to suppose that tectonic styles were different from those that shape contemporary crustal evolution - but how much and in what way? During the last decades, this discussion has been polarized between two schools of thought. One proposes a style of plate tectonics similar to the modern Earth, generally referred to as “horizontal” tectonics, in which crustal evolution is the result of convergent boundary processes such as subduction or collision. The other interprets Archaean geology in terms of a “stagnant” or “sluggish” regime with no or poor lateral mobility of the lid, in which crustal evolution is chiefly controlled by gravity-driven redistribution within the crust (“sagduction”) (e.g. Goodwin and Smith 1980) or “partial convective overturn” (e.g. Collins, Van Kranendonk, and Teyssier 1998), hence referred to as “vertical” tectonics.

However, recent developments in numerical modelling, as well as comparison with tectonic processes on the telluric planets, led to the realization that regarding “horizontal” and “vertical” tectonics as diametrically opposed is not an appropriate framework to understand Archean tectonic processes. On one hand, recent numerical models, as well as comparison with planets (e.g. Venus) emphasize the possibility of regional horizontal mobility, with locally divergent (rift) and convergent (“subduction-like”) domains that are not linked to a global system of plate boundaries (e.g. Hansen and Willis 1996; Harris and Bédard 2014). On the other hand, the development of internally consistent models for global tectonics, i.e. not restricted to crust, and/or without strongly prescribed boundary conditions, shows that partial convective overturn (“sagduction”) is actually hard to achieve for the melt-depleted lower crust, and lithospheric mantle is actually too stiff to permit crust-to lithosphere-wide Partial Convective Overturn (PCO) (Capitanio et al. 2011). This echoes recent structural studies of cratons, showing that whereas there is undoubtedly a component of gravity-driven instability in the strain patterns of the Archaean crust, it is superimposed on – and, quite often, minor compared to– a component of transpressive to bulk shortening deformation, accommodated by strain partitioning between vertical, often conjugate strike-slip shear zones (in the gneisses) and flattening with vertical extrusion (in the greenstones) (e.g. Chardon, Gapais, and Cagnard 2009; Zibra et al. 2014. How these processes link across scales and are reconciled within the global planetary regime remains outstanding (e.g. Korenaga 2018).

Global tectonics is, ultimately, the manifestation of the thermal state of the Earth. There are, however, only a few direct records of Earth’s thermal state. One of the rare proxies available is the metamorphic record. Mineral assemblages in equilibrium in a rock of given composition vary with pressure (P) and temperature (T). By combining the information from different metamorphic assemblages, it is commonly possible to reconstruct a portion of the PT conditions followed by the rock unit investigated. It is, furthermore, possible to date metamorphic assemblages. This is done by dating the crystallization age of a mineral (e.g. apatite, zircon) and linking it precisely to a metamorphic reaction and an assemblage. This approach, known as petrochronology, is now at the forefront of research in petrology (Engi, Lanari, and Kohn 2017; Lanari et al. 2019).

The Limpopo region, in South Africa, offers a unique opportunity to understand the timing and conditions of Archaean metamorphism because it exposes rocks formed at different structural levels from South to North.(i) an amphibolite-facies domain of gneisses and greenstones, part of the Kaapvaal Craton ; (ii) an upper amphibolite to granulite facies zone ; (iii) a granulite facies domain. The latter two are classically interpreted as forming the Southern Marginal Zone of a neo-Archaean (ca. 2.71-2.67 Ga), modern-style Limpopo orogeny, that is supposed to have thrust the high-grade Limpopo belt onto the Kaapvaal craton (D. Van Reenen et al. 1992). The upper amphibolite zone, in this model, is regarded as being formed of granulites from the nappe, retrogressed by fluids from the foreland, and is therefore usually called the Hydrated Zone. However, recent works bring new data that may not be compatible with this model. (i) Some high-grade mineral assemblages from the « granulite zone » of the Limpopo belt give ages as young as 2.0 Ga, i.e. 600 MYr younger than the proposed orogeny N. Madlakana, G. Stevens, and Bracciali 2020 ; (ii) melt features in the « granulite zone » give a range of age from 2.92 to 2.71 Ga (Vezinet et al. 2018), highly suggestive of multiple (or long-lived) metamorphic events in granulite facies conditions ; (iii) the age (and nature) of rocks in the « nappe » and in the « foreland » are exactly identical, clearly at odds with an allochthonous model (e.g. Laurent et al. 2011).

This study concerns the upper amphibolite to granulite facies zone from the South Marginal Zone. It is focused on the metapelites from the Bandelierkop Formation. This formation, and the metapelites, in particular, are rocks that concentrated most of the effort in research in the SMZ, even though it represents a small volume of the rocks (e.g. Nonkuselo Madlakana and Gary Stevens 2018; G. Stevens 1997; G. Nicoli et al. 2015). This is essentially because metapelites allow gaining great insight into the P-T conditions that the rocks undergone, as the aluminous minerals they bear are well constrained, such as garnet or cordierite (e.g. Bucher and Grapes 2011).

The goal was to carry out a preliminary work to try to show or not if these rocks were retrogressed from granulite facies, or had never reached those conditions. For that, one week of fieldwork was led to collect samples and a petrological study was realised on them. Thermodynamic modelling was conducted from XRF analysis to define PT conditions with an emphasis on the impact of fluid compositions on the equilibria. Due to the Covid-19, the dating of rutile and apatite by U/Pb to date the metamorphic events, that was supposed to be the core of this internship, could not be achieved and the petrology study has to be concentrated in 2 weeks of work before a precipitated return in France. The abbreviations used for this report are from Whitney and Evans 2010.

II. Geological settings and fieldwork

The NE-SW trending Limpopo belt delimits the Zimbabwe craton at the north from the Kaapvaal craton at the south and is situated at the border between South Africa, Botswana and Zimbabwe. This 300×200 km mobile belt is composed of high-grade metamorphic rocks and is interpreted as the result of the collision between the Kaapval craton and the Zimbabwe craton.

This belt can be delimited in three parts, from north to south: the North Marginal Zone (NMZ), the Central Zone (CZ) and the Southern Marginal Zone (SMZ) with each zone being delimited by major shear zones (A, Figure 1). These three parts have in common a metamorphic granulite facies but don't share the same geodynamic history, at least prior to ca. 2.0 Ga as the CZ has a polymetamorphic history, with 2 events at ca. 3.1 Ga and ca. 2.0 Ga (Kröner et al. 1999) which are both not recorded in the NMZ and the SMZ. Hence, the NMZ and the SMZ are usually reattached to their respective adjacent craton with lithologies similar to them, and the CZ as an independent terrane (DU TOIT, VAN REENEN, and ROERING 1983).

The SMZ is in contact with the northern part of the Kaapvaal Craton at the south via the north dipping Hout River Shear Zone and via the CZ at the north with the mostly vertical Palala Shear Zone (Roering et al. 1992). The lithologies are commonly regrouped in three main groups: (i) the grey granitoid gneiss complex, which forms the basement and the majority of the SMZ with mostly three ages of formation with 3457 ± 10, 3188 ± 6 and 2803 ± 11 Ma (Vezinet et al. 2018) and named the Baviaanskloof Gneiss Formation, (ii) the supracrustal rocks, which are bodies composed by meta-sediments, mostly metapelites and Banded Iron Formation (BIF), and (ultra)metabasite and known as the Bandelierkop Formation (BF), (iii) the intrusive plutons, mostly the Matok pluton (ca. 2.69 Ga) (e.g. Zeh, Gerdes, and Barton 2009 and the alkali shield complex (ca. 2.05 Ga), which overlap the two previous formations and postdate them (B, Figure 1).

In addition, the SMZ is traditionally subdivided into two metamorphic sub-zones, with granulite facies at the north and amphibolite facies at the south. The limit is commonly represented as an orthoamphibole isograd that overlay at the west with the N'Tabala Shear Zone (B, Figure 1). The southern part has been originally interpreted as a rehydrated zone, allowing retrogression from granulite facies to amphibolite facies (D. D. Van Reenen 1986). Hence this area is commonly named the Hydrated Zone (HZ).

Nevertheless, not recent works have been published on the metapelites from the HZ, and the effort has been focused on the metapelites from the granulite facies part (e.g. N. Madlakana, G. Stevens, and Bracciali 2020; Gautier Nicoli 2015). As a consequence, one week of fieldwork was organized to better understand the area and collect samples. 28 samples from the BF were taken, mainly metapelites, which will be the focus of this report. Their locality is reported in B, Figure 1 and a summary of their description and naming system is present in Annexe 2. The outcrops in this area are relatively scarce, as a consequence of the subtropical climate and the vegetation, and lots of samples come from loose blocks.

In terms of petrology at the macroscopic scale, the metapelites are usually caracterized by a assemblage of Grt, Oam, Qz, Pl and Bt. The Grt are most of the time centimetric and euhedral (A, Figure 3) and the Oam in form of black centimetric fibrous minerals (B, Figure 3). The samples closer to the Oam-isograd show most of the time presence of anatexis with leucosomes and restites (C, Figure 3), whereas this is less predominant for samples further south. Another difference between the two, is the presence of a texture of Grt surrounding a symplectic of Oamp+Ky+Pl±Crd close to the N'Tabala Shear Zone, which is not describe in the Litterature (D, Figure 2).

From this work and the samples collected, a petrographic study and thermodynamic modelling were led and chemical analysis were made.

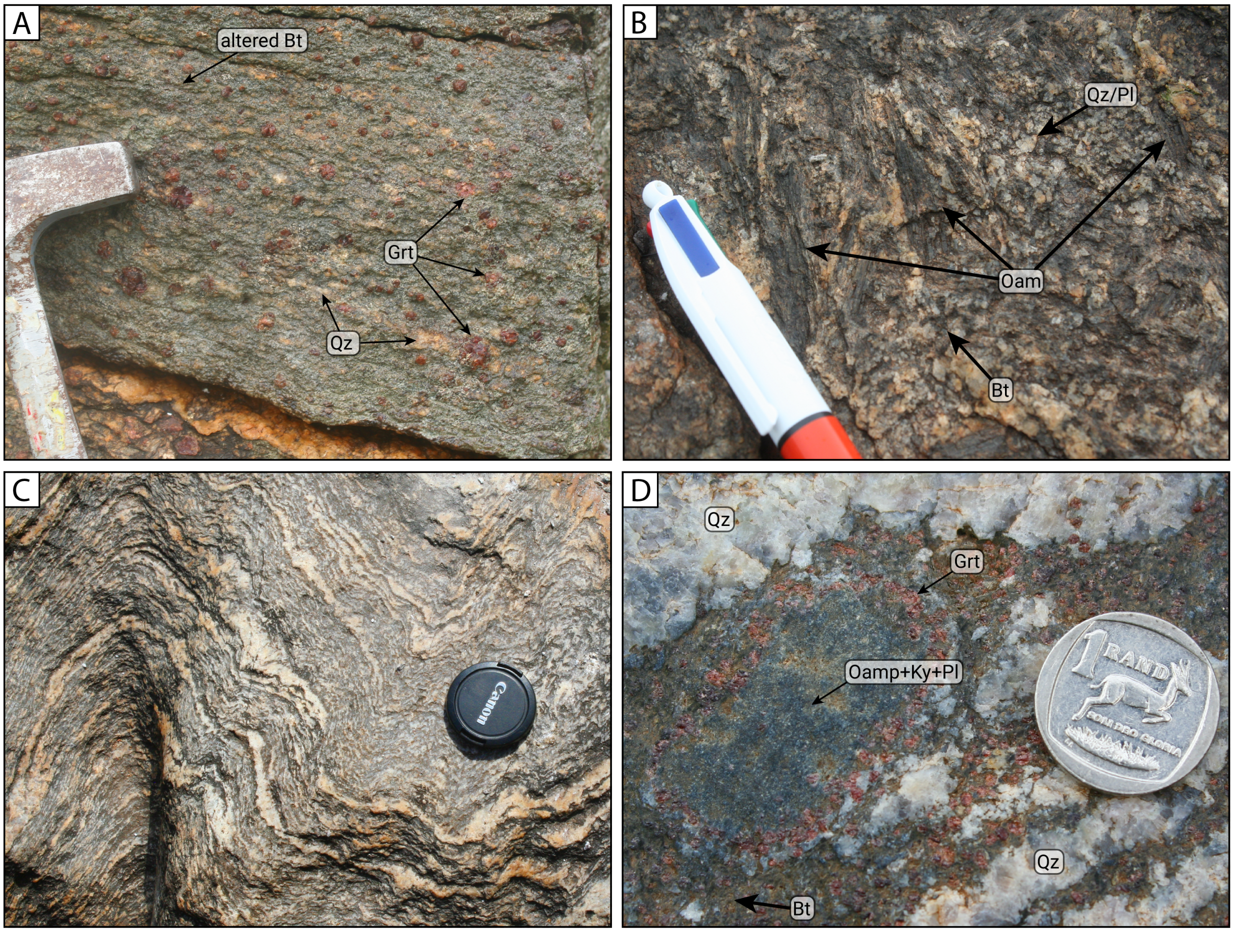

Figure 2: A) Photography of a metapelite far from the isograd showing the euhedral millimetric to centimetric Grt, outcrop HD02. B) Photography of a metapelite far from the isograd showing the Oam in form of centimetric fibrous black minerals, outcrop HD02. C) Photography of the anatectic and deform metapelite close to the isograd, outcrop HD12. D) Texture of coronitic Grt around a symplectic of Oamp+Ky+Pl, outcrop HD14.

III. Petrographic study and chemical analysis

One thin and one thick sections were made from each of the 28 samples. The samples were first investigated using a conventional petrographic microscope. Then, a ZeissEVO®Analytical Scanning Electron Microscope (SEM) from the Stellenbosch University Central Analytical Facilities was used to have high-resolution images. The analytical conditions were an acceleration voltage of 20 kV with a working distance of 8.5 mm, a specimen beam current of -20 nA. The same instrument was used to analyse major element compositions of the minerals present using energy-dispersive X-ray spectroscopy (EDS) with a 10 s counting time. Analyses were quantified using natural mineral standards. The detection limits for the Major elements range from $\pm$ 0.05 to 0.1 wt%.

Additionnally, the 22 samples of metapelites were crushed to a fine powder using a jaw crusher and tungsten swing mill, before the preparation of a fused disc for major element analysis. Bulk-rock chemistry was obtained by X-ray fluorescence (XRF) analysis using a PANalytical Axios Wavelength Dispersive spectrometer at the Central Analytical Facility at Stellenbosch University (results in Table 3 in appendix).

Three samples, HD02b, HD10b and HD12b, have been chosen to be the focus of the study. It is based on two criteria: a different distance from the O-amphibole isograd (orange triangles in Figure 1), and a similar bulk composition to be able to compare them (Table 1). These samples will be called HD02b HZ, HD12b Intermediate and HD10b Isograd, to show their relative distance from the isograd for the rest of this report.

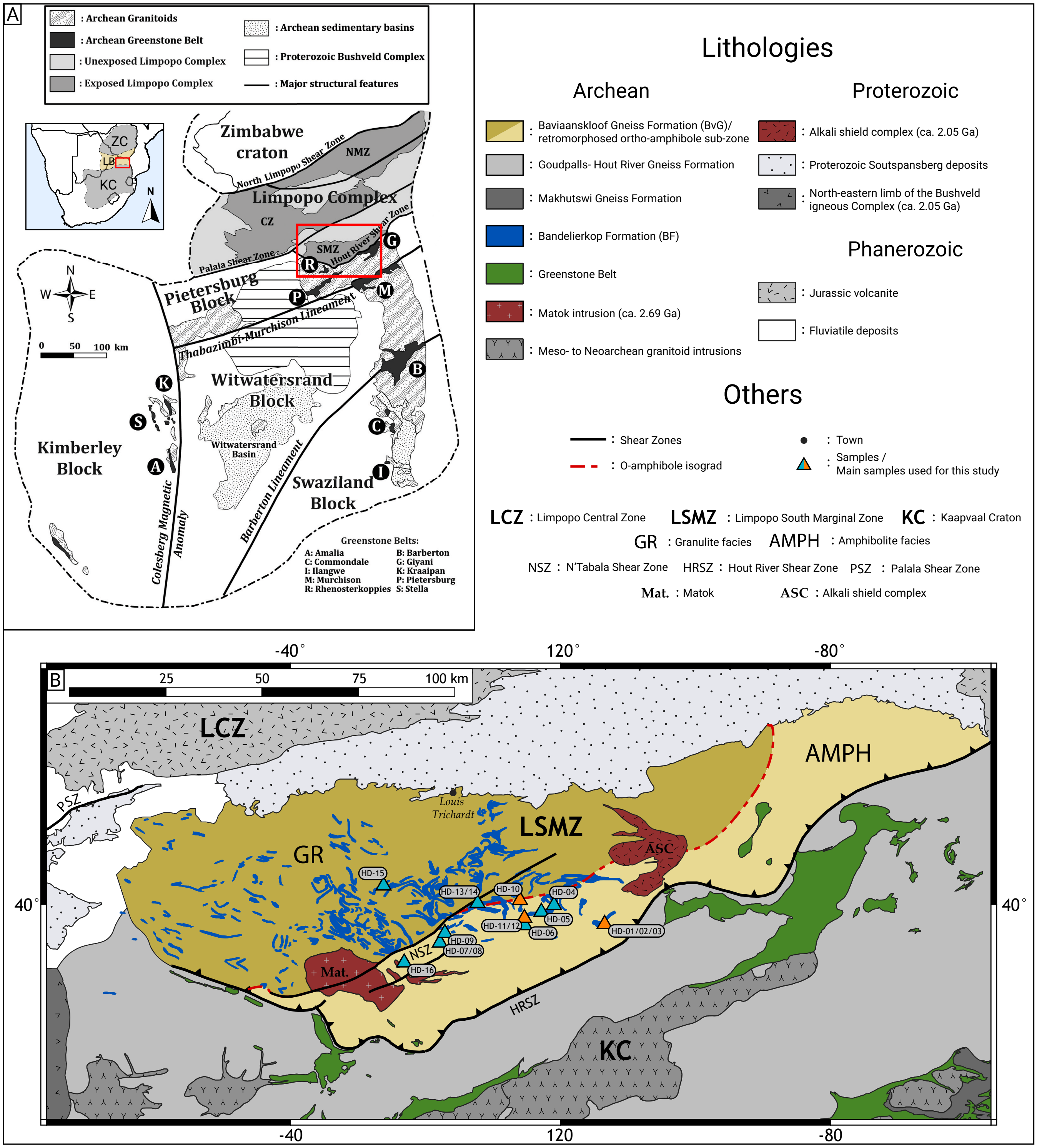

Figure 1: A) Simplified geological map of the Kaapvaal Craton and the northern terranes (modified from Eglington and Armstrong 2004; Poujol et al. 2003 and Vezinet et al. 2018). The red rectangle corresponds to B. Abbreviations: KC , Kaapvaal Craton ; LB , Limpopo Belt ; ZC , Zimbabwe Craton ; NMZ , Northern Marginal Zone ; CZ , Central Zone ; SMZ, Southern Marginal Zone. B) Simplified geological map of the Limpopo Southern Marginal Zone, from Brandl 1986 and Vezinet 2016. The isograd is from D. D. Van Reenen 1986. The triangles correspond to the samples from the fieldwork.

Sample name	Al_2O_3 (wt%)	CaO (wt%)	Cr_2O_3 (wt%)	FeO (wt%)	K_2O (wt%)	MgO (wt%)	MnO (wt%)	Na_2O (wt%)	P_2O_5 (wt%)	SiO_2 (wt%)	TiO_2 (wt%)	Mg#	A/CNK	Correction factor (%)
HD02b HZ	16.61	1.83	0.07	8.1	1.77	5.16	0.11	2.34	0.07	61.94	0.65	53.17	1.83	-
HD10b Isograd	17.18	1.4	0.11	8	1.83	7.48	0.09	1.69	0.06	59.68	0.6	62.49	2.35	-
HD12b Intermediate	15.02	2.14	0.12	9.84	2.2	7.63	0.12	2.59	0.06	57.89	0.68	58	1.43	-
HD02b HZ corrected	16.34	1.9	0.08	5.86	1.97	5.09	0.06	2.61	0.08	65.28	0.72	60.72	2.52	9
HD10b Isograd corrected	17.19	1.44	0.12	6.7	2	7.56	0.05	1.84	0.07	62.38	0.65	66.76	3.26	6.66
HD12b Intermediate corrected	14.72	2.15	0.12	8.17	2.43	7.92	0.06	2.87	0.07	60.74	0.75	63.32	1.97	7.92

Table 1: Table of bulk rock compositions of HD02b HZ, HD10b Isograd and HD12b Intermediate, from XRF analysis and corrected compositions without Grt1 and Grt2, with calculated Mg#, A/CNK and corrected factor.

Metapelites contain usually 0.2-1 cm-sized euhedral Grt poikiloblasts in a matrix of Bt, Qz, Oamp and Pl with essentially accessory Py, Ap, Mnz, Znr, Ilm and Ru (A in Figure 3). 0.2-1 cm-sized symplectic textures containing Oamp+Ky+Pl±Cor are also present (D in Figure 3). Grt are Almandine-rich and contain mostly Qz inclusions, with also Ilm, Oamp and sometimes Rt (B in Figure 3). Additionally, Gr is also present in some of the samples, in the matrix, and in Grt but not in the ones studied here (e.g. E from sample HD08a in Figure 3). Oamp has not been well constrained and is supposed to be similar to previous studies, with both anthophyllite and gedrite (e.g. G. Stevens 1997).

In all samples, it is possible to distinguish at least three generations of Grt (Grt1, Grt2 and Grt3), whether in terms of texture or chemical composition.

Grt1 composed the core of the grain, is euhedral, and contains usually small inclusions (< 50 μm). Grt2 has bigger but scarer inclusions and is also euhedral. Grt3 is at the rim of the Grt and is slightly different, with sub-euhedral small grains and small inclusions, mostly Qz but sometimes Ky, in a needle shape (B and C in Figure 3 and C and D in Figure 4).

In terms of chemical composition, the Rim-Rim cross-section from Figure 5, shows that Grt1 is chemically unzoned. Grt1 is chemically zoned, with enrichment of XFe and depletion of XMg at the rim and Grt3 is also chemically zoned, with an increase of XCa and a decrease of XFe, XMgo and XMn. Overall, the composition of Grt3 is slightly more calcic than Grt1 and Grt2.

These characteristics are observed for the three samples, whether in terms of texture or in terms of chemical composition.

The chemical analysis of the Grt for all the samples are reported in Figure 6. Each point of each generation for the point analysis come from a different grain. It shows a similar behaviour for HD02b HZ and HD10b Isograd, with continuity between Grt1 and Grt2 and a rupture with Grt3, due to an increase of Grs. Grt1 and Grt2 in HD12b Intermediate are more split, with small variations of Grs between the points. Concerning Grt3, it is similar to the two other samples and shows a gap with the 2 previous generations.

The Core-rim analysis shows the same evolution, with an increase of Alm for HD02b HZ between Grt1 and Grt2, an increase of Pyrope for the same Grt for HD10b Isograd and a more complicated path for HD12b Intermediate. Grt3 marks again a difference with the two previous generations, with an increase of Grs.

In terms of absolute composition, the bulk rock Mg# shows that it is too different between the samples to compare them.

Concerning the differences between samples, HD02b HZ and HD10b Isograd both host the symplectic texture of Oamp+Ky+Pl replacing Cor (D in Figure 3). But for HD10b Isograd, this texture is also around Grt, replacing Grt1 and Grt2 (D in Figure 4). This texture is not in HD12b Intermediate, but 0.5-1 cm sized Oam are present (A in Figure 4).

IV. Phase equilibria modelling: constraint on the P-T conditions and study of C-O-H fluids

To constrain the P-T conditions of the stable metamorphic phase assemblage present in the samples, phase equilibria modelling was made. Another reason was to try to better understand the influence of graphite-saturated-C-O-H (GCOH) fluids, in terms of redox state and equilibrium on the rocks studied. There is no graphite present in the 3 samples used, but graphite has been observed for an important part of the other samples collected (E in Figure 3 for instance). This presence shows the existence of C bearing fluids for a no- negligible part of the HZ and is then an important topic to understand for future work.

In modern metamorphic petrology, internal consistent databases of mineral properties (e.g. Holland and Powell 1998) have allowed making isochemical phase diagrams, also called pseudosections, by the use of forward modelling. The advantage of such an approach is that pseudosections are then applicable to a fixed bulk rock composition, for instance, an individual rock sample.

In this case, the XRF analyses need beforehand to be corrected. This is because all minerals are not in equilibrium with each other in the samples studied. In particular, Grt1 and Grt2 are not in equilibrium with the matrix and Grt3. This is chiefly shown by different texture and different chemical composition in Figure6 for instance, and by the fact that Grt is a mineral well known to be preserved in mineral assemblages. It is then important to take them into account, and to try to remove them from the bulk rock composition measured by XRF (Table 1). Bi shows an homogeneous composition and it seems also to be the case for Pl and Oam, from some few grains analysed. Hence, Grt is the only mineral that need to be removed.

To do that, the surface of Grt2 and Grt3 was measured from both the thin and thick sections for each sample. In was then used to calculate a ratio for the total surface occupied by Grt2 and Grt3 over the total surface of the sample, and it was then weighed over the real surface of the thin and thick section. It is then supposed to be representative of the whole rock collected in the field.

To achieve that, a script to measure surfaces was used on Illustrator (with Mordy Golding 2010 as shown in Figure 7. The Qz inclusions were removed from the grains, as they can represent an important surface. It is possible because SiO_2 is naturally in excess in metapelites, hence, it will not impact the models if it is slightly overestimated.

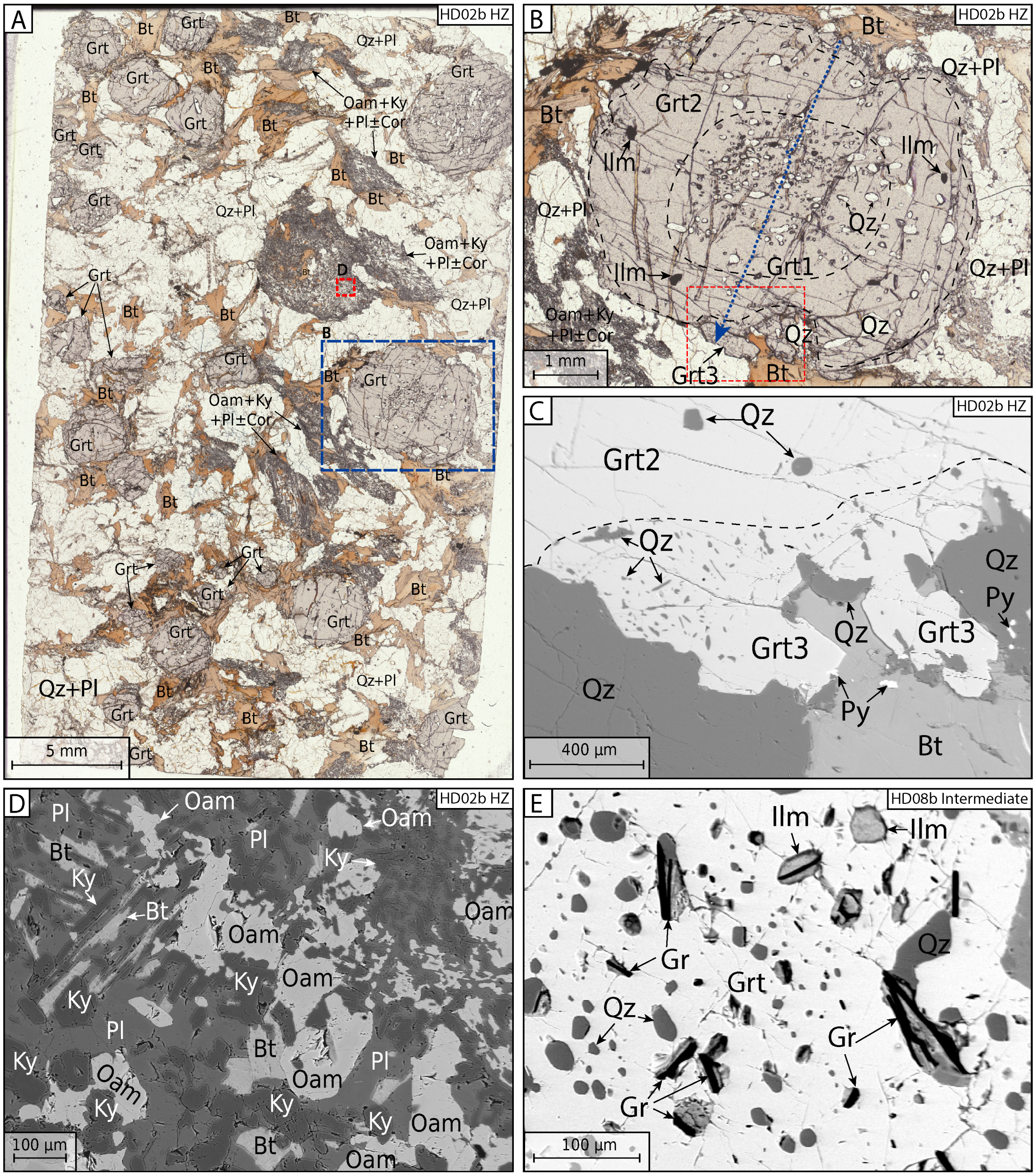

Figure 3: A) Scan of a thin section from the sample HD02b SMZ showing an overview of the main minerals and textures of the rock. The blue rectangle corresponds to B and the red rectangle to D. B) Zoom of A from sample HD02b SMZ, showing with black dotted lines the three generations of garnet (Grt1, Grt2 and Grt3) with their respective texture. A euhedral Grt1 with a poikilitic texture with mostly small quartz, a euhedral Grt2 with a similar poikilitic texture but with bigger quartz. The texture of Grt3 is shown in C. The red rectangle corresponds to C and the blue dotted arrow to the cross-section of the Figure 5. C) Back-scattered electron (BSE) image from SEM, showing the texture of the sub-anhedral Grt3, with small inclusions of quartz, in the form of a needle texture from sample HD02b SMZ. D) Back-scattered electron (BSE) image from SEM, showing the symplectic texture of Oamp, Ky and Pl with Bt in a replaced Crd. E) Back-scattered electron (BSE) image from SEM, showing the presence of graphite inside a garnet in sample HD08a Intermediate. All the abbreviations are from Whitney and Evans 2010.

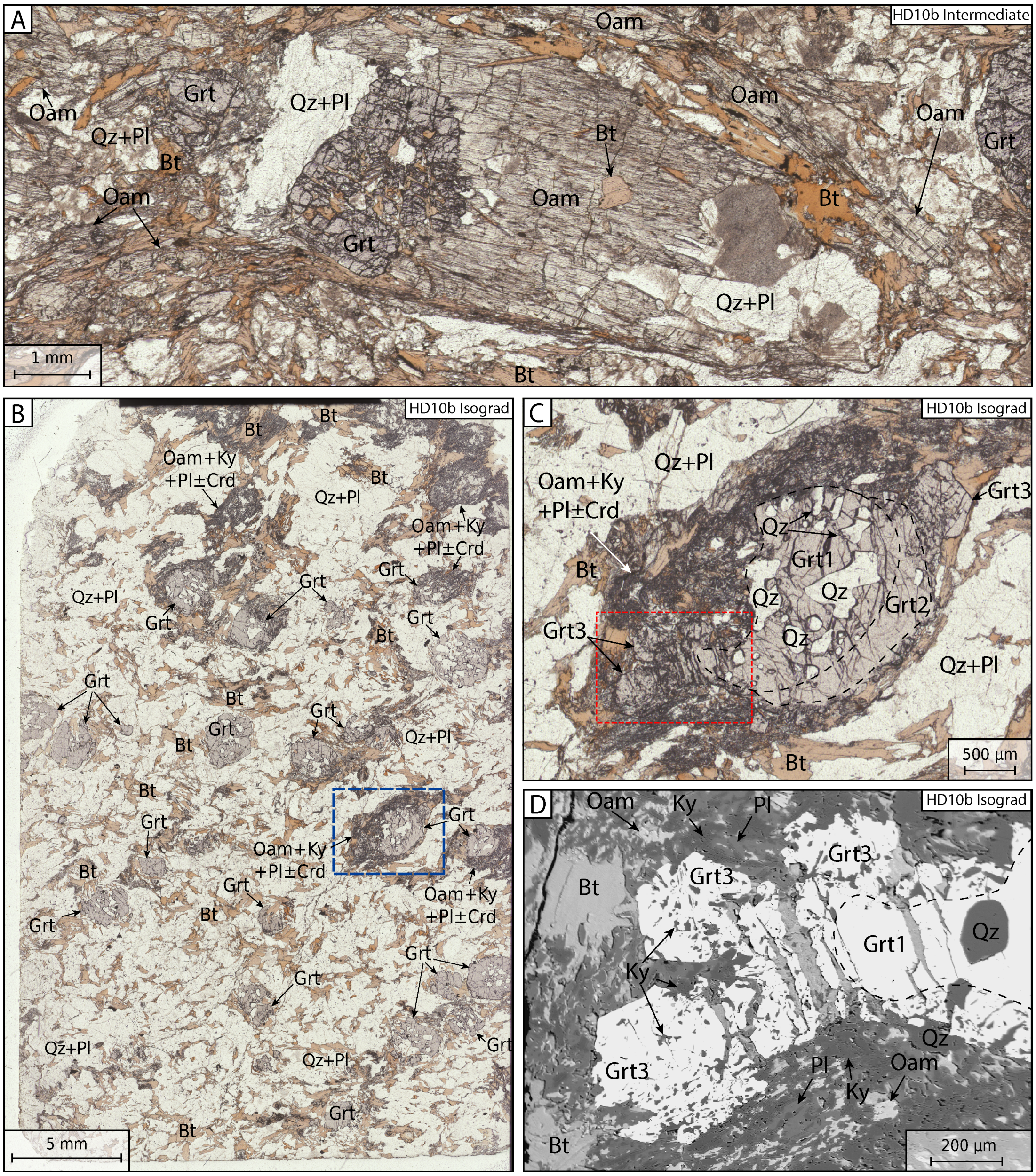

Figure 4: A) Zoom of a scan of a thin section from the sample HD12b Intermediate, showing the Oam B) Scan of a thin section from the sample HD10b Isograd showing an overview of the main minerals and textures of the rock. The blue rectangle corresponds to B. C) Zoom of B from sample HD10b Isograd, showing the three generations of garnet (Grt1, Grt2 and Grt3) with their respective texture, similar to B from 3. Grt3 and a symplectic texture of Ky, Oam and Pl is replacing Grt1. The red rectangle corresponds to C. D) Back-scattered electron (BSE) image from SEM, showing the euhedral Grt3 over Grt1, in the symplectic texture.

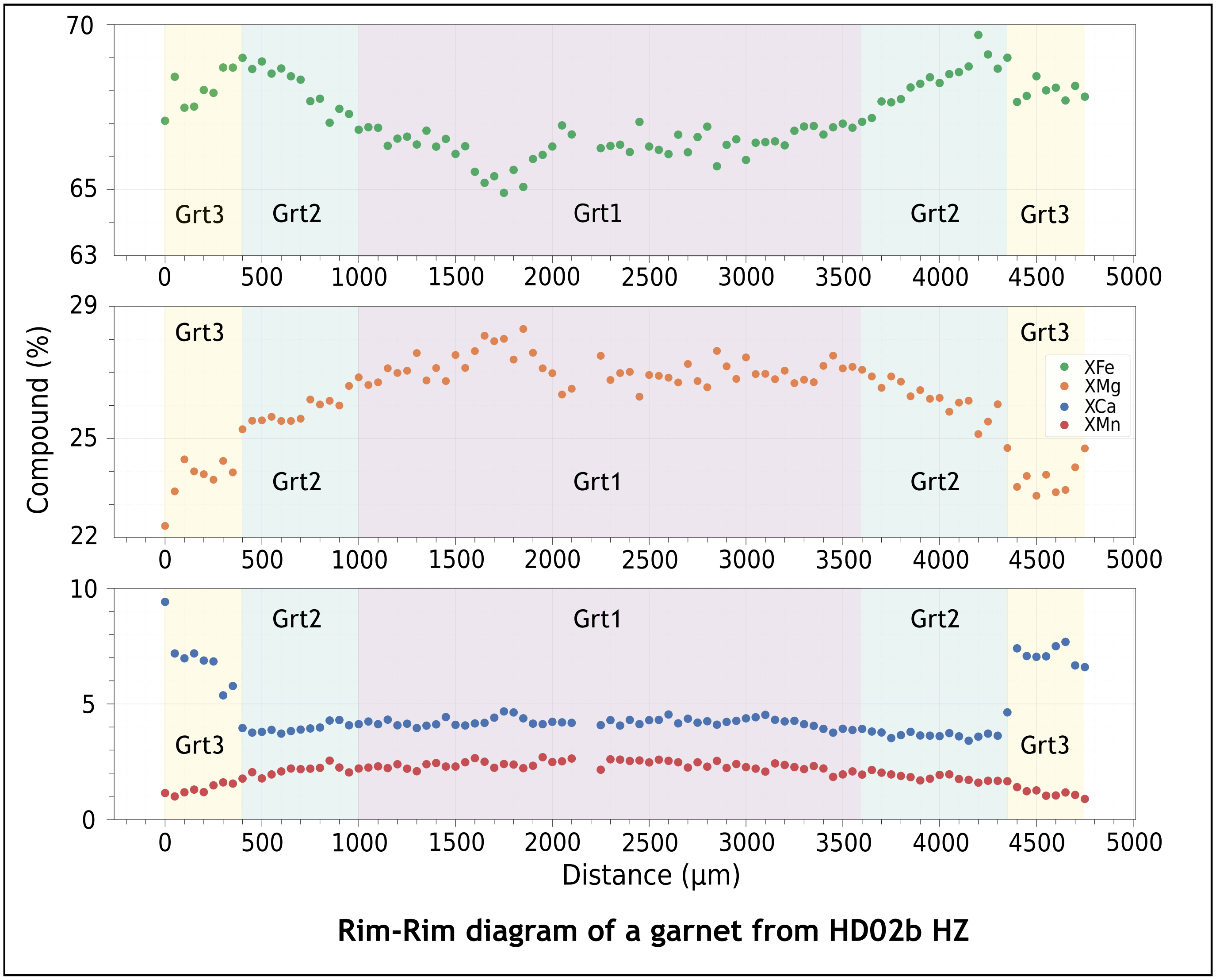

Figure 5: Rim-rim chemical cross-sections from EDS for the main poles of the garnet from sample HD02b SMZ in B in Figure 3, showing the three generations of garnet. Grt1 shows mostly no zonation, Grt2 is depleted in XMgO and enriched in XFeo and Grt3 is enriched in XCaO and depleted in XFeO, XMgO and XMn.

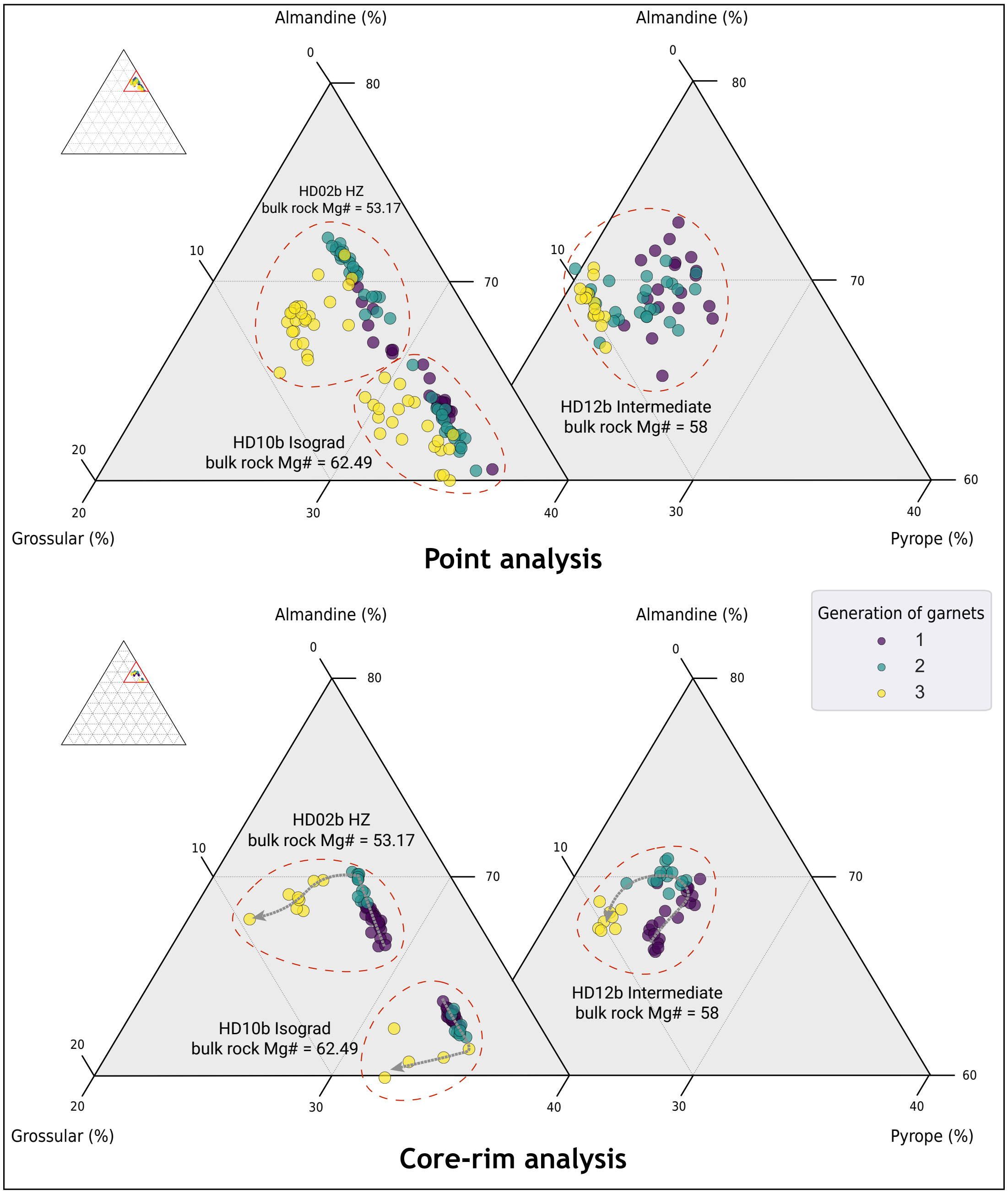

Figure 6: Garnet composition in a pyrope(XMg)-almandine(XFe)-grossular(XCa) ternary diagram from three different samples, HD03b, HD10b and HD12b. The three generations, similar to Figure 3, are shown in a different color. The first diagram corresponds to point analysis, with each point from each generation coming from a different garnet. The second diagram corresponds to three core-rim analysis on one grain made from each sample. The grey dotted arrows represent the path from the core to the rim. The #Mg corresponds to the bulk rock composition.

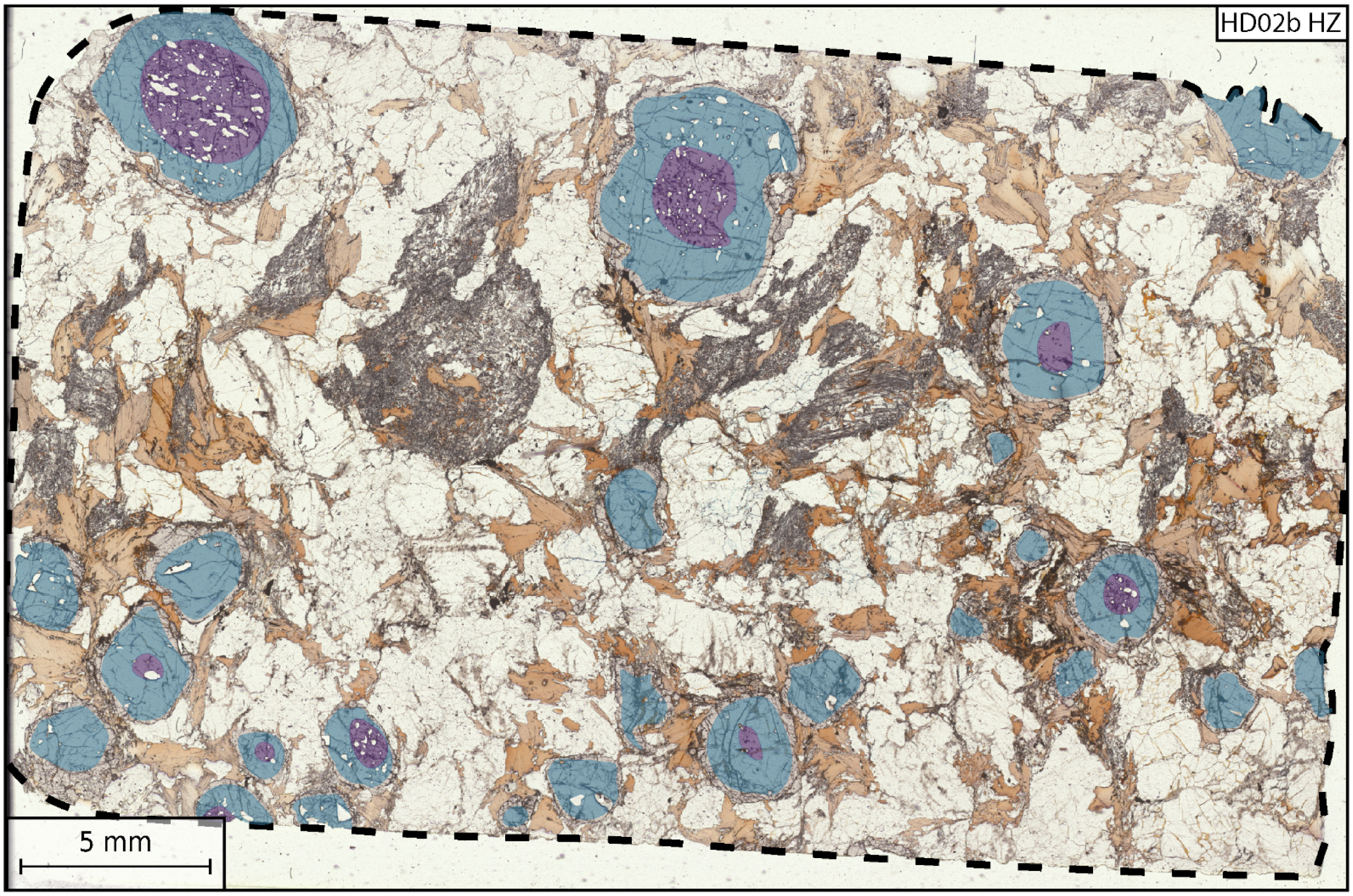

Figure 7: Scan of a thin section from HD02b SZM (same as A in 3), showing the surfaces measured for Grt1 (in purple) and Grt2 (in blue). The dotted line surface corresponds to the total surface of the thin section used.

With the ratio measured for the three samples, the corresponding composition from Grt1 and Grt2 was then removed from the previous bulk composition measured from XRF analysis. The result is shown in Table 1.

For the modelling, the software used was Perplex (version 6.8.9, April 2020, J. a. D. Connolly 1990). The chemical systems are MnO-Na_2O-CaO-K_2O-FeO-MgO-Al_2O_3-SiO_2-H_2O-TiO_2 (MnNCKFMASHT) and MnO-Na_2O-CaO-K_2O-FeO-MgO-Al_2O_3-SiO_2-H_2O-TiO_2-O_2-$2-CO$ (MnNCKFMASHTOC). The thermodynamic datafile used is hp62ver.dat. Solid solution models are: Mica(W), Bi(W), Gt(W), Opx(W), Melt(W), Crd(W), Chl(W) (R. W. White et al. 2014), feldspar (Fuhrman and Lindsley 1988), oAmph(DP) (Diener and Powell 2012) and Ilm(WPH) (White et al. 2000).

The approach was, for each sample, to calculate two pseudosections. One, with H_2O as a fluid and a second with GCOH fluids, to understand how it impacts the assemblages et reactions. To do that, the first pseudosection was calculated in the MnNCKFMASHT system, with the addition of an arbitrary value of 7wt% to the bulk composition to put the water in excess. For the second pseudosection, the MnNCKFMASHTOC system was used, with H_2O and CO_2 as saturated components, $X(O) = 1/3$ and the use of the Internal Equation of State modified Redich−Kwong equation from J. a. D. Connolly and Cesare 1993.

X(O) is defined as:

$$X(O) = \frac{N_O}{N_O + N_H}$$

With N_O and N_H being respectively the number of atoms of O and H. It is introduced first by Labotka 1991, and is a variable that is correlated with the redox state as $f(O_2)$, but has the advantage to directly reflects the mass balance and to be compositionally measurable in a fluid (J. A. D. Connolly 1995). In terms of value, X(O)

= 0 means pure CH_4 and X(O) = 1 means pure CO2 for a GCOH fluid, because of the projection through C. The value of 1/3 reflects the highest proportion of water in the fluid. It is also the value that is the most likely if there is no other constrain about the fluid composition, as dehydration reactions tend to dilute C during prograde path (e.g. Chu and Ague 2013). This is why this value was chosen for the pseudosections. Before analysing the pseudosections, it is important to remember that the way that fluids were defined, with an excess of H_2O or saturation of H_2O and CO_2 with X(O) = /3, is inaccurate with melting reactions, and that post-solidus reactions model here doesn't have any strong physical meaning. This is due to the overestimation of the water content with the coexistence of melt. The six pseudosections are presented in Figure 8.

The pseudosections show some similarities between samples, in particular, HD02b HZ and HD10b Isograd. HD12b Intermediate is slightly different, with the absence of Al_2O_5. This is nevertheless coherent with the absence of the symplectic texture containing Ky in HD12b. The assemblage corresponding to the samples, is Pl Grt Bt Oam Ky Qz Rt H2O/fluid for HD02b and HD10b, and Pl Grt Bt Oam Qz Rt H2O/fluid for HD10b.

Concerning the effect of GCOH fluids, the more important change concerns the position of the solidus, as it is shifted to higher P and T. This is coherent as this reflect a decrease of the activity of H_2O ($a(H_2O)$) in the fluid. This is even more pronounced at lower P, as the $a(H_2O)$ is lower at these conditions (Chu and Ague 2013). In addition, GCOH fluids also impact the formation of Ti oxides, as it is dependant on the redox state, because of the iron. It allows the formation of assemblages where Rt and Ilm are coexisting, like in HD02b SMZ type for example.

To try to constrain better the P-T conditions of the assemblage present in the samples, composition isopleths of the four poles of Grt were computed and are represented in Figure 9. The bold lines represent the median composition of Grt3 from the analytical part for each sample. At the exception of HD02b HZ type, the isopleths don't seem to overlap in the assemblage of interest. In particular, Almandine seems particularly low. It is expected concerning the pseudosections with GCOH fluids, as there is no Gr in the samples, and therefore no proof of C in the system. It is not the case concerning HD12b and HD10b with H_2O in excess, with the intersection of the isopleths that seem to exist in the Pl Chl Grt Bt Oamp Qz Rt H2O ±Ky even though Chl has not been observed in the petrology study in the fresh rock. Nevertheless, HD02b HZ shows PT conditions of ca. 650 °C for ca. 8.5 kbar.

V. Discussion and conclusion

The HZ metapelites seem to record different PT conditions, with clearly three different generations of Grt. The Grt1 record no chemical zoning, in agreement with retrogression from granulite facies, as stated in previous studies (e.g. G. Stevens 1997). In addition, Grt1 and Grt2 seem in continuity with each other, but it is not the case with Grt3, both in terms of texture and chemical composition. The relations of the textures in HD10b (C and D in Figure 4) have shown that Grt1 and Grt2 have been replaced by Cor. This is also well described in the Litterature (e.g. Gary Stevens and van Reenen 1992; D. D. Van Reenen 1986). In addition, Cor is replaced by a symplectic texture of Oamp+Ky+Pl, in equilibrium with Bt and Grt3, as demonstrated with the Ky inclusions in it and the relations between the two. This has important implications in terms of PT conditions and suggests that Grt3 are retrogressed Grt, with Grt1 and Grt2 preserving peak metamorphism conditions. Furthermore, Grt1 shows no chemical zoning, which is consistent with a granulite facies.

In addition, the thermodynamic modelling has shown for HD02b HZ PT conditions of ca. 650 °C for ca. 8.5 kbar, and it seems to be a good sample to continue with modelling. These PT conditions are consistent with previous works on the retrograde assemblage on the HZ (e.g. D. D. Van Reenen 1986). Concerning HD10b Isograd and HD12b Intermediate, the isopleths didn't overlap and it can be explained by different reasons: there are lots of pyrite in the samples, which may represent a non-negligible amount of Fe. The chemical system used here doesn't take into account sulphites and it may explain the inaccuracy of the isopleths. It may also be that the correction of the bulk composition was not accurate and not representative of the samples studied.

The pseudosections with GCOH fluids have shown that this composition has an important impact concerning the solidus, with a shifting of an addition of around

HD02b (SMZ type) SiO$_2$ 65.39 TiO$_2$ 0.73 Al$_2$O$_3$ 16.37 FeO 5.87 MgO 5.10 CaO 1.91 Na$_2$O 2.61 K$_2$O 1.98 (wt%)

MnNCKFMASHTO with 7 wt% of H$_2$O MnNCKFMASHTOC with H$_2$O+CO$_2$+Gr saturated and X(O) = 1/3

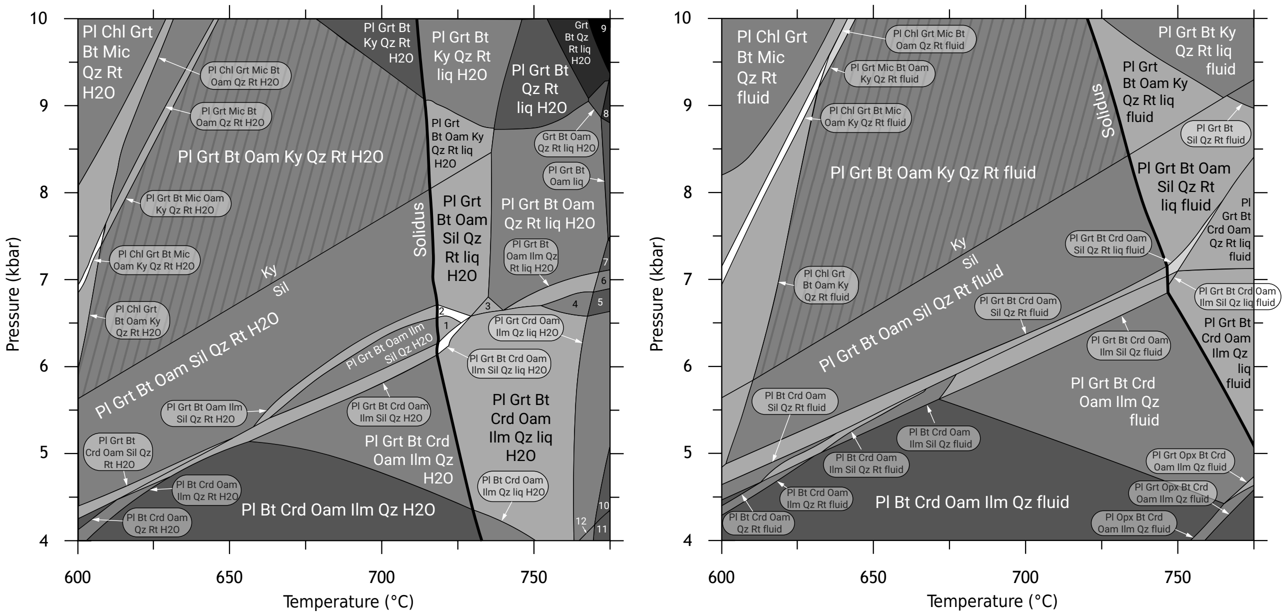

(1) Pl Grt Bt Oam Ilm Sil Qz liq H2O (2) Pl Grt Bt Oam Ilm Sil Qz Rt liq H2O (3) Pl Grt Bt Crd Oam Qz Rt liq H2O (4) Pl Grt Bt Oam Ilm Qz liq H2O (5) Pl Grt Oam Ilm Qz liq H2O (6) Pl Grt Oam Ilm Qz Rt liq H2O (7) Pl Grt Oam Qz Rt liq H2O (8) Grt Bt Oam Qz Rt liq (9) Grt Bt Qz Rt liq (10) Pl Grt Crd Oam Ilm liq H2O (11) Pl Opx Crd Oam Ilm liq H2O (12) Pl Opx Crd Oam Ilm Qz liq H2O

HD12b (intermediate type) SiO$_2$ 60.90 TiO$_2$ 0.75 Al$_2$O$_3$ 14.75 FeO 8.19 MgO 7.93 CaO 2.16 Na$_2$O 2.87 K$_2$O 2.44 (wt%)

MnNCKFMASHTO with 7 wt% of H$_2$O MnNCKFMASHTOC with H$_2$O+CO$_2$+Gr saturated and X(O) = 1/3

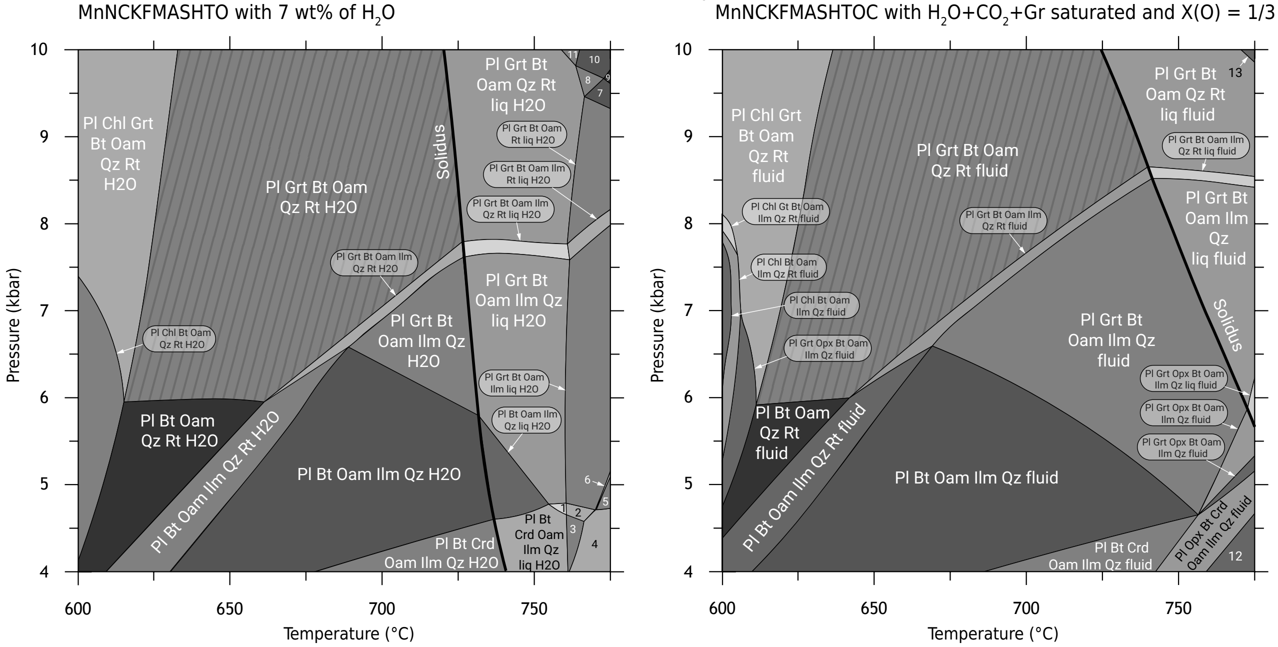

(1) Pl Grt Bt Crd Oam Ilm Qz liq H2O (2) Pl Grt Bt Crd Oam Ilm liq H2O (3) Pl Bt Crd Oam Ilm liq H2O (4) Pl Opx Bt Crd Oam Ilm liq H2O (5) Pl Opx Bt Oam Ilm liq H2O (6) Pl Grt Opx Bt Oam Ilm liq H2O (7) Pl Grt Bt Oam Rt liq (8) Pl Grt Bt Oam Qz Rt liq (9) Grt Bt Oam Rt liq (10) Grt Bt Oam Qz Rt liq (11) Grt Bt Oam Qz Rt liq H2O (12) Pl Opx Bt Crd Ilm Qz fluid (13) Grt Bt Oam Qz Rt liq fluid

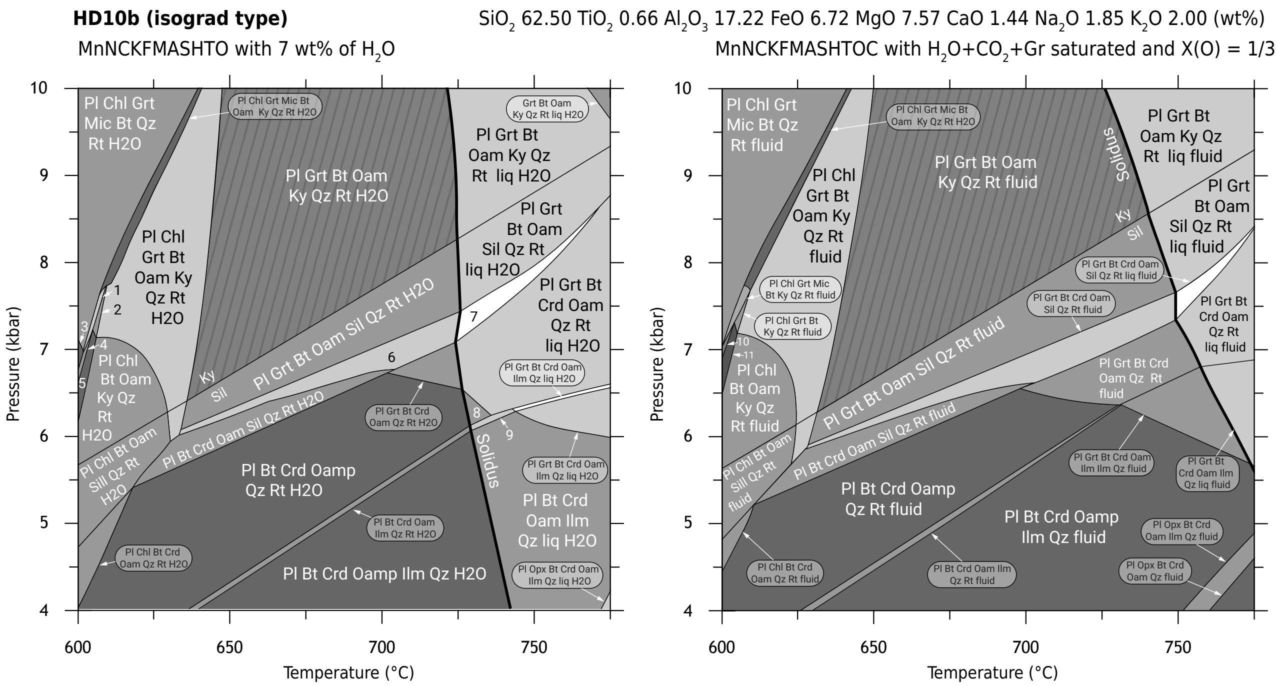

(1) Pl Chl Grt Mic Bt Ky Qz Rt H2O (2) Pl Chl Grt Bt Ky Qz Rt H2O (3) Pl Chl Mic Bt Qz Rt H2O (4) Pl Chl Mic Bt Ky Qz Rt H2O (5) Pl Chl Bt Ky Qz Rt H2O (6) Pl Grt Bt Crd Oam Sil Qz Rt H2O
(7) Pl Grt Bt Crd Oam Sill Qz Rt liq H2O (8) Pl Bt Crd Oam Qz Rt liq H2O (9) Pl Bt Crd Oam Ilm Qz Rt liq H2O (10) Pl CHl Mic Bt Ky Qz Rt fluid (11) Pl Chl Bt Ky Qz Rt fluid

Figure 8: Calculated P-T pseudosections from the corrected bulk composition. The bulk composition and the conditions of the system are at the top of each pseudosection. The inferred mineralogical assemblage is indicated by a diagonally shaded field.

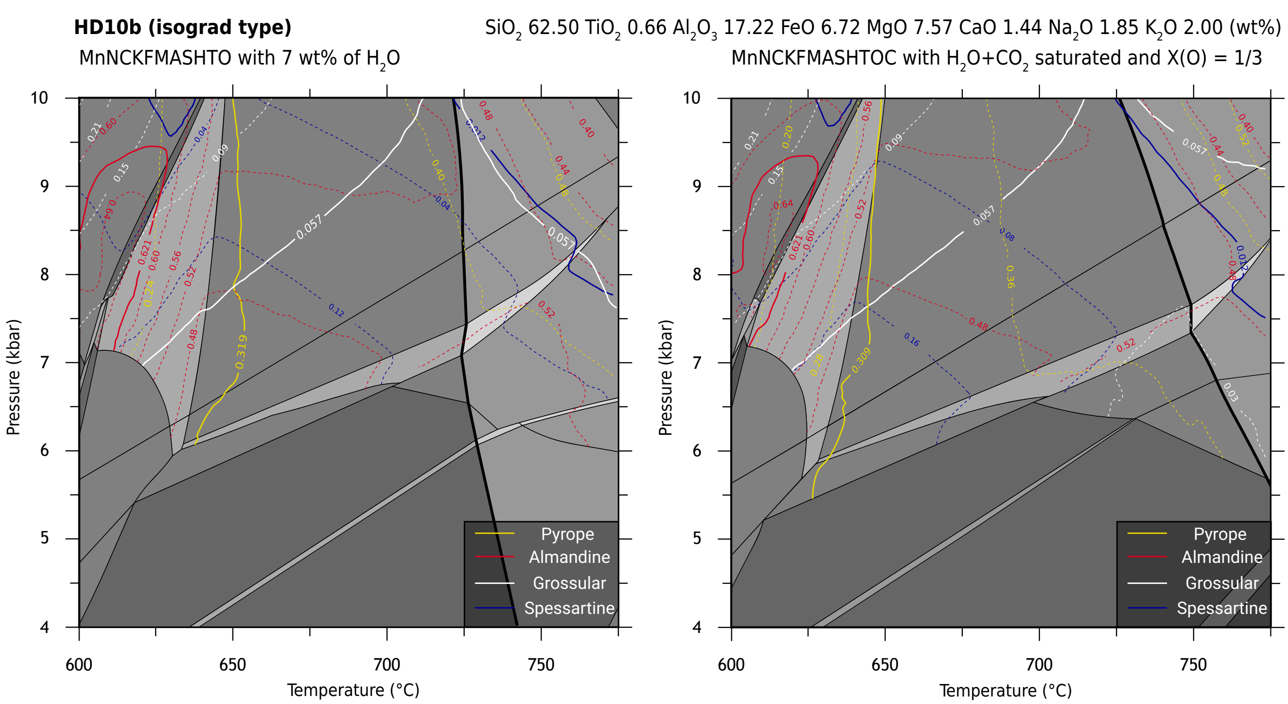

Mediane composition of Grt3 from HD10b : 62.07 % Almandine, 30.92 % Pyrope, 5.67 % Grossular, 1.18 % Spessartine

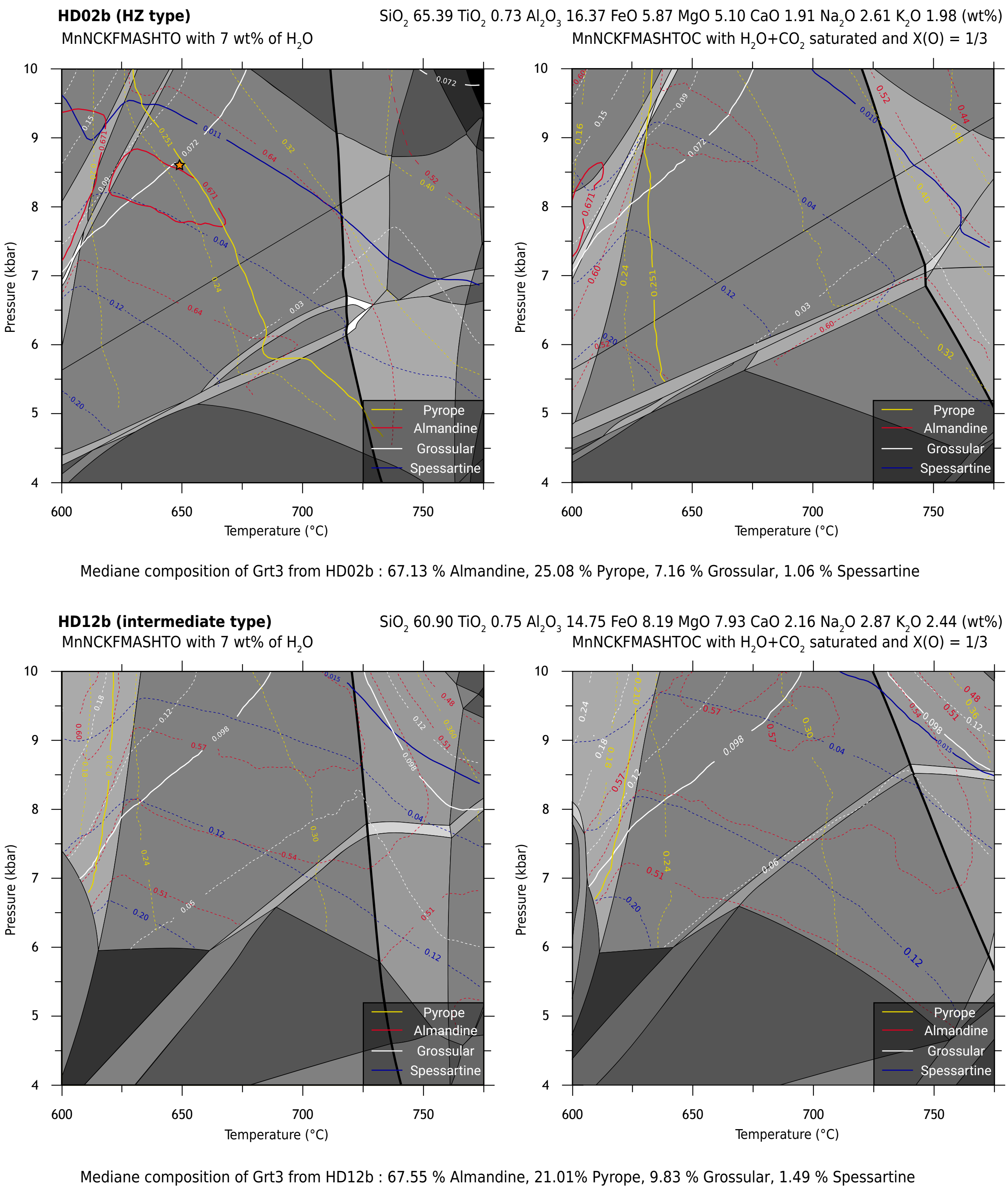

Figure 9: Calculated isopleths (mol %) for garnet poles. The bold lines correspond to the composition of the median of Grt3 from each sample, measured previously. These values are at the bottom of each pseudosection. The bulk composition and the conditions of the system are at the top of each pseudosection. The orange star represents the possible PT conditions for HD02b HZ.

75° C at low pressure before melting. Nevertheless, the consequences at the PT conditions of interest are not so important, as the pseudosections are quite similar, at the exception of the Ti oxides. Nevertheless, it may be important to use samples containing graphite, to be able to compare with something real.

With the elements collected, it is possible to formulate a hypothesis concerning the history of these rocks: peak metamorphism in granulite facies, recorded in the core Of the Grt1, with an absence of zonation, a decompression event, with the replacement of Grt1 and Grt2 by Cor and a cooling down event, with the current assemblage and Grt3 replacing Cor. This is in accordance with recent work on the other sides of the isograde where approximately the same PT conditions where found (N. Madlakana, G. Stevens, and Bracciali 2020). It may reflect that they recorded the same metamorphic event but with different degrees of fluid availability. This would explain the absence of Opx in this HZ, as stated in previous works (e.g. D. Van Reenen et al. 1992).

To try to answer that question, the next step of this work would be to try to date metamorphism by geochronology as it was first planned for this internship. The best approach would be to do in situ dating, to be able to date the different generations of Grt, by Ap or Rt, as they are quite present in the samples. The petrology study can also be improved, as Oamp have not been studied, which can help to better constrain the PT conditions. Additionally, the spatial representativeness can be greatly improved, as it was only focused on three samples. Furthermore, it would be important to try to model the PT conditions of Grt1 and Grt2, to confirm or not the hypothesis formulated. A way to do that would be to progressively remove the composition of Grt1 and Grt2 during a PT loop to try to reproduce the complete story of the rocks.

Acknowledgments

I would like to thank Gary Stevens, for this internship and for his availability to answer my dumb questions, even with the exceptional situation. It was quite a ride, with all the logistic problems linked to the epidemic, but I did try my best to make science in this context. My gratitude also goes towards Jean-François Moyen, for his presence and his invitation for the field trip, it was a dream come true to walk on a craton for me. Finally, my thanks to James Connolly for the modelling part and the useful discussions about fluids.

References

Brandl, Günther (1986). *The Geology of the Pietersburg Area: Explanation of Sheet 2328, Scale 1: 250 000*. Republic of South Africa, Department of Mineral and Energy Affairs . . .

Bucher, Kurt and Rodney Grapes (2011). "Metamorphism of Pelitic Rocks (Metapelites)". In: *Petrogenesis of Metamorphic Rocks*. Ed. by Kurt Bucher and Rodney Grapes. Berlin, Heidelberg: Springer, pp. 257–313. ISBN: 978-3-540-74169-5. DOI: 10.1007/978-3-540-74169-5_7.

Capitanio, F. A. et al. (Dec. 2011). "Subduction Dynamics and the Origin of Andean Orogeny and the Bolivian Orocline". In: *Nature* 480.7375, pp. 83–86. ISSN: 0028-0836, 1476-4687. DOI: 10.1038/nature10596.

Chardon, Dominique, Denis Gapais, and Florence Cagnard (Nov. 15, 2009). "Flow of Ultra-Hot Orogens: A View from the Precambrian, Clues for the Phanerozoic". In: *Tectonophysics*. Hot Orogens 477.3, pp. 105–118. ISSN: 0040-1951. DOI: 10.1016/j.tecto.2009.03.008.

Chu, X. and J. J. Ague (2013). "Phase Equilibria for Graphitic Metapelite Including Solution of CO2 in Melt and Cordierite: Implications for Dehydration, Partial Melting and Graphite Precipitation". In: *Journal of Metamorphic Geology* 31.8, pp. 843–862. ISSN: 1525-1314. DOI: 10.1111/jmg.12047.

Collins, W.J, M.J Van Kranendonk, and C Teyssier (Sept. 1998). "Partial Convective Overturn of Archaean Crust in the East Pilbara Craton, Western Australia: Driving Mechanisms and Tectonic Implications". In: *Journal of Structural Geology* 20.9-10, pp. 1405–1424. ISSN: 01918141. DOI: 10.1016/S0191-8141(98)00073-X.

Connolly, J. A. D. (Feb. 1, 1995). "Phase Diagram Methods for Graphitic Rocks and Application to the System C-O-H-FeO-TiO2-SiO2". In: *Contributions to Mineralogy and Petrology* 119.1, pp. 94–116. ISSN: 1432-0967. DOI: 10.1007/BF00310720.

Connolly, J. a. D. (Jan. 6, 1990). "Multivariable Phase Diagrams; an Algorithm Based on Generalized Thermodynamics". In: *American Journal of Science* 290.6, pp. 666–718. ISSN: 0002-9599, 1945-452X. DOI: 10.2475/ajs.290.6.666.

Connolly, J. a. D. and B. Cesare (1993). "C-O-H-S Fluid Composition and Oxygen Fugacity in Graphitic Metapelites". In: *Journal of Metamorphic Geology* 11.3, pp. 379–388. ISSN: 1525-1314. DOI: 10.1111/j.1525-1314.1993.tb00155.x.

Diener, J. F. A. and R. Powell (2012). "Revised Activity–Composition Models for Clinopyroxene and Amphibole". In: *Journal of Metamorphic Geology* 30.2, pp. 131–142. ISSN: 1525-1314. DOI: 10.1111/j.1525-1314.2011.00959.x.

DU TOIT, M.C, D. D. VAN REENEN, and C. ROERING (1983). "Some Aspects of the Geology, Structure and Metamorphism of the Southern Marginal Zone of the Limpopo Metamorphic Complex". In: *Some aspects of the geology, structure and metamorphism of the southern marginal zone of the Limpopo metamorphic Complex* 8, pp. 121–142. ISSN: 0367-5335.

Eglington, B. M. and R. A. Armstrong (June 1, 2004). "The Kaapvaal Craton and Adjacent Orogens, Southern Africa: A Geochronological Database and Overview of the Geological Development of the Craton". In: *South African Journal of Geology* 107.1-2, pp. 13–32. ISSN: 1012-0750. DOI: 10.2113/107.1-2.13.

Engi, Martin, Pierre Lanari, and Matthew J. Kohn (2017). "Significant Ages—An Introduction to Petrochronology". In: *Reviews in Mineralogy and Geochemistry* 83.1, pp. 1–12.

Fuhrman, Miriam L. and Donald H. Lindsley (Apr. 1, 1988). "Ternary-Feldspar Modeling and Thermometry". In: *American Mineralogist* 73.3-4, pp. 201–215. ISSN: 0003-004X. URL: https://pubs.geoscienceworld.org/ammin/article-abstract/73/3-4/201/42101/Ternary-feldspar-modeling-and-thermometry (visited on 05/29/2020).

Goodwin, A.M. and I.E.M. Smith (Feb. 1980). "Chemical Discontinuities in Archean Metavolcanic Terrains and the Development of Archean Crust". In: *Precambrian Research* 10.3-4, pp. 301–311. ISSN: 03019268. DOI: 10.1016/0301-9268(80)90016-9.

Hansen, Vicki L. and James A. Willis (Oct. 1996). "Structural Analysis of a Sampling of Tesserae: Implications for Venus Geodynamics". In: *Icarus* 123.2, pp. 296–312. ISSN: 00191035. DOI: 10.1006/icar.1996.0159.

Harris, Lyal B and Jean H Bédard (2014). "Crustal Evolution and Deformation in a Non-Plate-Tectonic Archaean Earth: Comparisons with Venus". In: *Evolution of Archean Crust and Early Life*. Ed. by Yildirim Dilek and Harald Furnes. Modern Approaches in Solid Earth Sciences. Dordrecht: Springer Netherlands, pp. 215–291. ISBN: 978-94-007-7615-9. DOI: 10.1007/978-94-007-7615-9_9.

Holland, T. J. B. and R. Powell (1998). "An Internally Consistent Thermodynamic Data Set for Phases of Petrological Interest". In: *Journal of Metamorphic Geology* 16.3, pp. 309–343. ISSN: 1525-1314. DOI: 10.1111/j.1525-1314.1998.00140.x.

Korenaga, Jun (2018). “Crustal Evolution and Mantle Dynamics through Earth History”. In: *Philosophical Transactions of the Royal Society A: Mathematical, Physical and Engineering Sciences* 376.2132, p. 20170408.

Kröner, A. et al. (Feb. 1, 1999). “Single Zircon Ages for Granitoid Gneisses in the Central Zone of the Limpopo Belt, Southern Africa and Geodynamic Significance”. In: *Precambrian Research* 93.4, pp. 299–337. ISSN: 0301-9268. DOI: 10.1016/S0301-9268(98)00102-8.

Labotka, Theodore C. (1991). “Chemical and Physical Properties of Fluids”. In: *Reviews in Mineralogy* 26, pp. 43–104.

Lanari, Pierre et al. (2019). “Metamorphic Geology: Progress and Perspectives”. In: *Geological Society, London, Special Publications* 478.1, pp. 1–12. ISSN: 0305-8719, 2041-4927. DOI: 10.1144/SP478-2018-186.

Laurent, Oscar et al. (Apr. 1, 2011). “Geochemistry and Petrogenesis of High-K “Sanukitoids” from the Bulai Pluton, Central Limpopo Belt, South Africa: Implications for Geodynamic Changes at the Archaean–Proterozoic Boundary”. In: *Lithos*. Secular Variations in Magmatism and Tectonic Implications 123.1, pp. 73–91. ISSN: 0024-4937. DOI: 10.1016/j.lithos.2010.12.009.

Madlakana, N., G. Stevens, and L. Bracciali (Feb. 1, 2020). “Paleoproterozoic Amphibolite Facies Retrogression and Exhumation of Archean Metapelitic Granulites in the Southern Marginal Zone of the Limpopo Belt, South Africa”. In: *Precambrian Research* 337, p. 105532. ISSN: 0301-9268. DOI: 10.1016/j.precamres.2019.105532.

Madlakana, Nonkuselo and Gary Stevens (2018). “Plagioclase Disequilibrium Induced during Fluid-Absent Biotite-Breakdown Melting in Metapelites”. In: *Journal of Metamorphic Geology* 36.9, pp. 1097–1116. ISSN: 1525-1314. DOI: 10.1111/jmg.12429.

Nicoli, G. et al. (2015). “Rapid Evolution from Sediment to Anatectic Granulite in an Archean Continental Collision Zone: The Example of the Bandelierkop Formation Metapelites, South Marginal Zone, Limpopo Belt, South Africa”. In: *Journal of Metamorphic Geology* 33.2, pp. 177–202. ISSN: 1525-1314. DOI: 10.1111/jmg.12116.

Nicoli, Gautier (Apr. 20, 2015). “The Metamorphic and Anatectic History of Archaean Metapelitic Granulites from the South Marginal Zone, Limpopo Belt, South Africa”. thesis. Saint-Etienne. URL: http://www.theses.fr/2015STET4021 (visited on 02/13/2020).

Poujol, M. et al. (Nov. 10, 2003). “A Review of the Geochronological Constraints on the Evolution of the Kaapvaal Craton, South Africa”. In: *Precambrian Research*. Archaean Tectonics, Volume 1 127.1, pp. 181–213. ISSN: 0301-9268. DOI: 10.1016/S0301-9268(03)00187-6.

Roering, C. et al. (Mar. 1, 1992). “Tectonic Model for the Evolution of the Limpopo Belt”. In: *Precambrian Research*. The Archaean Limpo Granulite Belt: Tectonics and Deep Crustal Processes 55.1, pp. 539–552. ISSN: 0301-9268. DOI: 10.1016/0301-9268(92)90044-O.

Stevens, G. (1997). “Melting, Carbonic Fluids and Water Recycling in the Deep Crust: An Example from the Limpopo Belt, South Africa”. In: *Journal of Metamorphic Geology* 15.1, pp. 141–154. ISSN: 1525-1314. DOI: 10.1111/j.1525-1314.1997.00010.x.

Stevens, Gary and Dirk van Reenen (Mar. 1, 1992). “Constraints on the Form of the P-T Loop in the Southern Marginal Zone of the Limpopo Belt, South Africa”. In: *Precambrian Research*. The Archaean Limpo Granulite Belt: Tectonics and Deep Crustal Processes 55.1, pp. 279–296. ISSN: 0301-9268. DOI: 10.1016/0301-9268(92)90028-M.

Van Reenen, D. D. (Aug. 1, 1986). “Hydration of Cordierite and Hypersthene and a Description of the Retrograde Orthoamphibole Isograd in the Limpopo Belt, South Africa”. In: *American Mineralogist* 71.7-8, pp. 900–915. ISSN: 0003-004X. URL: https://pubs.geoscienceworld.org/ammin/article-abstract/71/7-8/900/41890/Hydration-of-cordierite-and-hypersthene-and-a (visited on 05/05/2020).

Van Reenen, D.D. et al. (Mar. 1992). “Regional Geological Setting of the Limpopo Belt”. In: *Precambrian Research* 55.1-4, pp. 1–5. ISSN: 03019268. DOI: 10.1016/0301-9268(92)90009-D.

Vezinet, Adrien (Nov. 3, 2016). “Différenciation et Stabilisation de La Croûte Continentale Archéenne, l’exemple de La Marge Nord Du Craton Du Kaapvaal En Afrique Du Sud”. thesis. Lyon. URL: http://www.theses.fr/2016LYSES054 (visited on 02/13/2020).

Vezinet, Adrien et al. (Feb. 1, 2018). “A Record of 0.5 Ga of Evolution of the Continental Crust along the Northern Edge of the Kaapvaal Craton, South Africa: Consequences for the Understanding of Archean Geodynamic Processes”. In: *Precambrian Research* 305, pp. 310–326. ISSN: 0301-9268. DOI: 10.1016/j.precamres.2017.11.019.

White, R. W. et al. (2014). “New Mineral Activity–Composition Relations for Thermodynamic Calculations in Metapelitic Systems”. In: *Journal of Metamorphic Geology* 32.3, pp. 261–286. ISSN: 1525-1314. DOI: 10.1111/jmg.12071.

White et al. (Sept. 1, 2000). “The Effect of TiO2 and Fe2O3 on Metapelitic Assemblages at Greenschist and Amphibolite Facies Conditions: Mineral Equilibria Calculations in the System K2O-FeO-MgO-Al2O3-SiO2-H2O-TiO2-Fe2O3". In: *Journal of Metamorphic Geology* 18, pp. 497–511. DOI: 10.1046/j.1525-1314.2000.00269.x.

Whitney, Donna L. and Bernard W. Evans (Jan. 1, 2010). "Abbreviations for Names of Rock-Forming Minerals". In: *American Mineralogist* 95.1, pp. 185–187. ISSN: 0003-004X. DOI: 10.2138/am.2010.3371.

with Mordy Golding (2010). *Adobe Illustrator CS5 : For Web and Interactive Design*. Ventura, CA : Lynda.com, [2010] ©2010. URL: https://search.library.wisc.edu/catalog/9910101663502121.

Zeh, Armin, Axel Gerdes, and Jackson M. Barton (May 1, 2009). "Archean Accretion and Crustal Evolution of the Kalahari Craton—the Zircon Age and Hf Isotope Record of Granitic Rocks from Barberton/Swaziland to the Francistown Arc". In: *Journal of Petrology* 50.5, pp. 933–966. ISSN: 0022-3530. DOI: 10.1093/petrology/egp027.

Zibra, I. et al. (Oct. 2014). "On Shearing, Magmatism and Regional Deformation in Neoarchean Granite-Greenstone Systems: Insights from the Yilgarn Craton". In: *Journal of Structural Geology* 67, pp. 253–267. ISSN: 01918141. DOI: 10.1016/j.jsg.2013.11.010.

Appendix

Sample	GPS point (lat. ; long.)	Lithologies and additional description
HD-01a	(-23.3509639 ; 30.27259011)	Meta-BIF, in place
HD-01c	(-23.3509639 ; 30.27259011)	Ortho-amphibolite in place
HD-01d	(-23.3509639 ; 30.27259011)	Ortho-amphibolite in place
HD-02a	(-23.35191174 ; 30.2754653)	Metapelite in place
HD-02b	(-23.35191174 ; 30.2754653)	Metapelite, Bt rich in place
HD-02c	(-23.35191174 ; 30.2754653)	Metapelite, Oam rich in place
HD-03	(-23.35173097 ; 30.27492028)	Meta-arkose, in place
HD-04	(-23.3052959 ; 30.14809131)	Metabasite, loose block
HD-05	(-23.32053855 ; 30.11570998)	Metapelite, loose block with big Oam oxidized
HD-06	(-23.351405 ; 30.07340156)	Metapelite, loose block, Bt rich
HD-07a	(-23.38753775 ; 29.85687126)	Metapelite, loose block, presence of Crd
HD-07b	(-23.38753775 ; 29.85687126)	Metapelite, loose block, presence of Crd
HD-07c	(-23.38753775 ; 29.85687126)	Metapelite, loose block, euhedral Grt accumulation in gz-fsp matric
HD-08a	(-23.38302801 ; 29.85865134)	Metapelite, loose block, lot of Grt and Crd
HD-08b	(-23.38302801 ; 29.85865134)	Metapelite, loose block, lot of Grt and Crd
HD-09	(-23.36549907 ; 29.8702424)	Metapelite, loose block, layered Bt-Grt-Crd rock with leucosomes
HD-10a	(-23.29205562 ; 30.06225781)	Metapelite, in place, coarse grained
HD-10b	(-23.29205562 ; 30.06225781)	Metapelite, in place, fine grained
HD-11a	(-23.33406285 ; 30.07246681)	Breccia, with gneiss and sandstone
HD-11b	(-23.33406285 ; 30.07246681)	Metapelite, in place, coarse grain with Crd
HD-12a	(-23.33305648 ; 30.07296603)	Metapelite, in place, migmatitic metapelite andabundant Grt
HD-12b	(-23.33305648 ; 30.07296603)	Metapelite, in place, migmatitic Oam rich
HD-13a	(-23.29435084 ; 29.9545882)	Metapelite, in place, Crd rimmed with Grt
HD-13b	(-23.29435084 ; 29.9545882)	Metapelite, in place, Crd rimmed with Grt
HD-13c	(-23.29435084 ; 29.9545882)	Metapelite, in place, Crd rimmed with Grt
HD-14	(-23.29697504 ; 29.95468447)	Metapelite, in place, Crd rimmed with Grt
HD-15	(-23.25115807 ; 29.71765098)	Metapelite, in place, granulite facies with large Grt
HD-16	(-23.43222275 ; 29.76543139)	Migmatite, in place, Grt-Crd leucosome

Table 2: Table of the samples localisation and description, collected during fieldwork. Samples with the same number are from the same area.

Sample name	Al2O3 (wt%)	CaO (wt%)	Cr2O3 (wt%)	Fe2O3 (wt%)	K2O (wt%)	MgO (wt%)	MnO (wt%)	Na2O (wt%)	P2O5 (wt%)	SiO2 (wt%)	TiO2 (wt%)	Mg#	A/CNK
HD02a	16.61	1.77	0.13	9.68	2.02	7.75	0.09	2.22	0.06	57.88	0.68	61.32	1.83
HD02b	16.61	1.83	0.07	9.00	1.77	5.16	0.11	2.34	0.07	61.94	0.65	53.17	1.83
HD02c	18.11	1.32	0.15	7.09	2.64	7.39	0.09	1.90	0.09	59.42	0.64	67.36	2.16
HD05	15.63	2.13	0.12	8.42	0.92	6.97	0.10	2.96	0.07	60.98	0.61	62.11	1.60
HD06	17.49	1.67	0.10	6.92	1.97	6.31	0.04	2.13	0.08	60.99	0.55	64.36	2.02
HD07a	15.52	1.80	0.10	7.88	2.41	6.52	0.08	2.38	0.08	61.01	0.59	62.10	1.58
HD07b	17.06	1.45	0.13	10.18	2.52	8.57	0.10	2.11	0.04	55.81	0.74	62.50	1.93
HD07c	15.39	1.48	0.07	17.63	0.09	6.18	0.14	0.96	0.27	57.89	0.48	40.97	3.52
HD08a	12.85	4.21	0.06	18.22	0.04	5.38	0.20	0.25	0.39	57.84	0.33	36.90	1.58
HD08b	12.49	1.29	0.17	6.33	1.42	6.20	0.05	1.70	0.03	68.42	0.54	65.98	1.87
HD09	14.08	1.74	0.08	6.47	1.61	5.41	0.06	2.39	0.07	65.82	0.49	62.34	1.59
HD10a	16.42	1.84	0.11	7.90	2.00	6.84	0.06	2.34	0.08	60.26	0.66	63.16	1.75
HD10b	17.18	1.40	0.11	8.89	1.83	7.48	0.09	1.69	0.06	59.68	0.60	62.49	2.35
HD11b	12.00	4.12	0.06	18.48	0.74	4.79	0.14	0.36	0.04	57.09	0.40	33.92	1.35
HD12a	12.28	1.44	0.05	13.01	1.35	4.57	0.14	1.30	0.11	63.87	0.39	41.02	1.97
HD12b	15.02	2.14	0.12	10.94	2.20	7.63	0.12	2.59	0.06	57.89	0.68	58.00	1.43
HD13a	18.02	1.11	0.09	12.18	2.53	6.80	0.10	1.89	0.04	55.25	0.84	52.50	2.29
HD13b	17.07	1.71	0.08	9.92	2.37	5.54	0.08	3.08	0.06	57.43	0.74	52.51	1.59
HD13c	18.37	1.84	0.07	9.56	2.58	5.24	0.09	3.86	0.05	56.44	0.70	52.05	1.47
HD14	18.91	1.32	0.10	14.35	3.88	7.56	0.11	2.37	0.04	48.99	0.97	51.06	1.80
HD15	19.38	0.50	0.16	14.34	2.21	11.67	0.10	0.38	0.03	50.00	0.92	61.71	4.93
HD16	16.06	1.79	-	1.13	0.85	0.54	0.01	5.89	0.06	72.82	0.16	48.62	1.16

Table 3: Table of the bulk rock compositions of the metapelites from XRF analysis. Samples with the same number are from the same area.